Geophysical Research Letters

RESEARCH LETTER
10.1029/2018GL079255

Special Section:
Cassini's Final Year: Science Highlights and Discoveries

Saturn's Atmosphere at 1–10 Kilometer Resolution

Andrew P. Ingersoll[1], Shawn P. Ewald[1], Kunio M. Sayanagi[2], and John J. Blalock[2]

[1]Division of Geological and Planetary Sciences, California Institute of Technology, Pasadena, CA, USA, [2]Department of Atmospheric and Planetary Sciences, Hampton University, Hampton, VA, USA

Abstract We present images of Saturn from the final phases of the Cassini mission, including images with 0.5 km per pixel resolution, as high as any Saturn images ever taken. Notable features are puffy clouds resembling terrestrial cumulus, shadows indicating cloud height, dome and bowl shaped cloud structures indicating upwelling and downwelling in anticyclones and cyclones respectively, and filaments, which are thread-like clouds that remain coherent over distances of 20,000 km. From the coherence of the filaments, we give upper bounds on the diffusivity and kinetic energy dissipation. A radiative transfer analysis by Sanz-Requena et al. (2018) indicates that methane-band imagery is most useful in determining cloud and haze properties in the 60–250 mbar pressure range. Our methane-band imagery finds haze in this pressure range covering 64°-74°planetocentric latitude. Filaments lie within the haze, and cumulus clouds lie below it, but pressure levels are uncertain below the 250 mbar level.

Plain Language Summary During its final half-year, the Cassini spacecraft took close-up images from 3000–4000 km above Saturn's cloud tops. The spatial resolution was as high as any images ever taken of the planet. They revealed isolated puffy clouds like terrestrial cumulus and also more exotic, threadlike clouds - filaments - that would stretch halfway around the Earth if they were on our planet. The filamentary clouds indicate that the level of turbulence in Saturn's atmosphere is very low. The images showed dome-shaped clouds indicative of upwelling at the centers of anticyclones and bowl-shaped clouds indicative of downwelling at the centers of cyclones.

Key Points:
- Close-up imaging by the Cassini spacecraft reveals long filamentary clouds and puffy cumulus clouds at 0.5 km resolution
- A dome-shaped cloud structure in anticyclones suggests upwelling, and a bowl-shaped cloud structure in cyclones suggests downwelling
- Thread-like filamentary clouds 20,000 km long suggest a laminar flow with extremely low values of diffusivity and dissipation

Supporting Information:
- Supporting Information S1

Correspondence to:
A. P. Ingersoll,
api@gps.caltech.edu

Citation:
Ingersoll, A. P., Ewald, S. P., Sayanagi, K. M., & Blalock, J. J. (2018). Saturn's atmosphere at 1–10 kilometer resolution. *Geophysical Research Letters*, *45*, 7851–7856. https://doi.org/10.1029/2018GL079255

Received 30 MAR 2018
Accepted 13 JUL 2018
Accepted article online 24 JUL 2018
Published online 11 AUG 2018

1. Introduction

On 29 November 2016, the Cassini mission began its F-ring proximal orbit (FRPO) phase, which consisted of highly inclined orbits crossing the equatorial plane near periapse from north to south on the day side. The F-ring orbits, in which periapse lay just outside the rings, continued until 23 April 2017, at which time the proximal orbits began. Periapse on these orbits lay inside the rings, 3000–4000 km above the clouds. There were 22 proximal orbits, the last of which ended with the final plunge into Saturn's atmosphere on 15 September 2017. Since northern summer solstice occurred on 24 May 2017, the FRPO phase was ideal for high-resolution imaging of high northern latitudes. We present a sample of images from 2016 and 2017 taken mostly with the wide-angle camera (WAC) of the imaging science subsystem (ISS) (Porco et al., 2004). The WAC has a shorter exposure time for the same signal-to-noise ratio than the narrow-angle camera (NAC). To avoid motion blur, only the WAC was used on the proximal orbits. The resolution ranged from tens of km per pixel over the pole to 0.5 km per pixel over the equator. To focus on images at the highest possible resolution, we restrict our analysis to latitudes lower than the hexagon, which is centered at 75±1°N (All latitudes in this paper are planetocentric).

Vasavada et al. (2006) presented polar stereographic projections of Saturn's south polar region on 18 September 2004, during Cassini's first revolution of the planet. Image resolution was 50 km/pixel. They noted ubiquitous "patchy" clouds that extend from 84°S to 60°S. The patchy clouds exist in both hemispheres. Dyudina et al. (2009) measured the rotation of the patchy clouds from 70°S to 85°S and found them to be anticyclones with relative vorticity ζ of -1×10^{-4} rad s^{-1}. Antunano et al. (2018) call them "puffy" clouds with sizes from 10 to 500 km. The puffy/patchy clouds are invisible in the methane filters, so they are not part of the optically thin haze. Antunano et al. (2018) say the clouds are probably of convective origin. Consistent with the words patchy and puffy, we will call them cumulus clouds based exclusively on their morphology and the dictionary definition "a class of clouds characterized by dense individual elements in the form of puffs, mounds, or towers with tops that often resemble cauliflower." The word cumulus is derived from the Latin word for a heap or pile, and we use it simply because it matches the clouds' appearance.

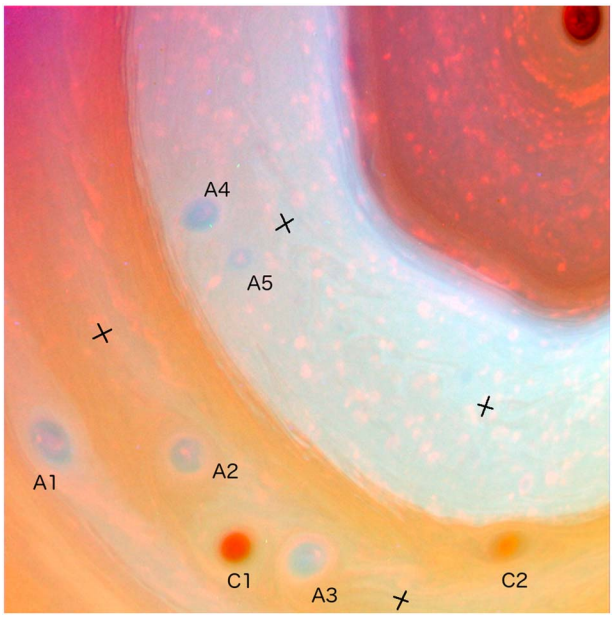

Figure 1. False-color methane band image used to estimate cloud heights. Red indicates deep cloud below clear atmosphere. White and blue indicate high cloud or haze. Crosses are at 60°N and 70°N, and at 130°W and 175°W. Anticyclones and cyclones are labeled with the letters A and C, respectively. The same features appear in Figures 2 and 3 of this paper. The images were taken on 7 March 2017 with the wide-angle camera at a resolution perpendicular to the boresight of 30 km/pixel. The Sun is at the upper right. Image numbers and further details are in the SI.

Section 2 discusses methane band imagery and what it says about the heights of clouds within the vortices at latitudes of 55–65°N. These are the same vortices whose evolution from 2007 to 2016 was chronicled by del Rio-Gaztelurrutia et al. (2018). Because of the higher resolution, our work complements theirs. Section 3 discusses cloud heights derived from cloud shadows, both within the vortices and in the filamentary regions. The filaments and cumulus clouds are discussed in Section 4. Based on the coherence of the filaments over large distances, in Section 5 we place rough upper bounds on the horizontal diffusivity and kinetic energy dissipation. Section 6 has a summary including unanswered questions.

2. Methane Band Imagery

Figure 1 shows a methane band image of Saturn's northern hemisphere taken during the F-ring orbits. North–south distance along the 1-bar surface between the crosses is 9678 km. The east–west distances along the surface are 14,765 km and 21,864 km at latitudes of 70°and 60°, respectively. The "eye" of the polar cyclone is the prominent red spot in the upper right corner. It extends from the pole down to 88.5°N. Two corners and three sides of the hexagon occupy the region 75 ± 1°N. Filters and their central wavelengths include CB2 (752 nm), MT2 (728 nm), and MT3 (890 nm). The figure uses red for the CB2 image, green for the MT2 image, and blue for the MT3 image. The color balance was chosen to make the band between 74°N and 64°N look white. Since methane gas is a strong absorber in MT3 and a moderate absorber in MT2, deep clouds below a clear atmosphere will look red. Conversely, clouds at high altitude will look white. An optically thin haze layer above a deep cloud will have bright features of the deep cloud showing through as pink and dark features showing through as light blue.

Sanz-Requena et al. (2018) used VIO, BL1, MT2, CB2, and MT3 images from 26 June 2013 to study haze and cloud heights around Saturn's north pole. They use a full radiative transfer model, which is beyond the scope of the present paper largely because we have only broad-band CB2 and CLR filters and little or no angular coverage. The greatest sensitivity to cloud properties comes where the methane filters have intermediate optical depths - where the transmission to space is around 0.5, for example. Sanz-Requena et al. (2018) estimate that the MT2 and MT3 filters have greatest sensitivity to cloud properties at altitudes between 60 mbar and 250 mbar, and they cite West et al. (2009) and Garcia-Melendo et al. (2009, 2011) for earlier estimates. They also state that the CB2 filter is sensitive to an intermediate region of tropospheric haze at 350–700 mbar as well as the region down to the tropospheric cloud deck at 1.4 bars.

A semi-transparent haze occupies the region from 74°N to 64°N. Cumulus clouds exist at deeper levels, both inside and outside the hexagon. Figure S1 of the supporting information shows Figure 1 along with its three single-filter component images – CB2, MT3, and MT2. Although the color balance is arbitrary, the relative brightness across each single-filter image is not. Figure S2 shows the same scene in 2013. The relative brightness in the single-filter images indicates that the haze layer was largely absent in 2013. The red vortices C1 and C2 are cyclones, and the blue vortices A1 - A5 are anticyclones. Apparently the high cloud in the anticyclones is semi-transparent because it reveals puffy pink clouds below. The anticyclones A2 and A3 with the cyclone C1 in between constitute the ACA system that was tracked from 2012 through 2016 by del Rio-Gaztelurrutia et al. (2018).

3. Shadows and Shading

Figure 2 shows the cyclone C2, which lies to the north and east of the ACA system in Figure 1. The filter is CB2, which shows the main cloud deck, not an optically thin haze layer visible only in the methane filters. The Sun in the top three images is beyond the pole to the north. We interpret the filamentary features at

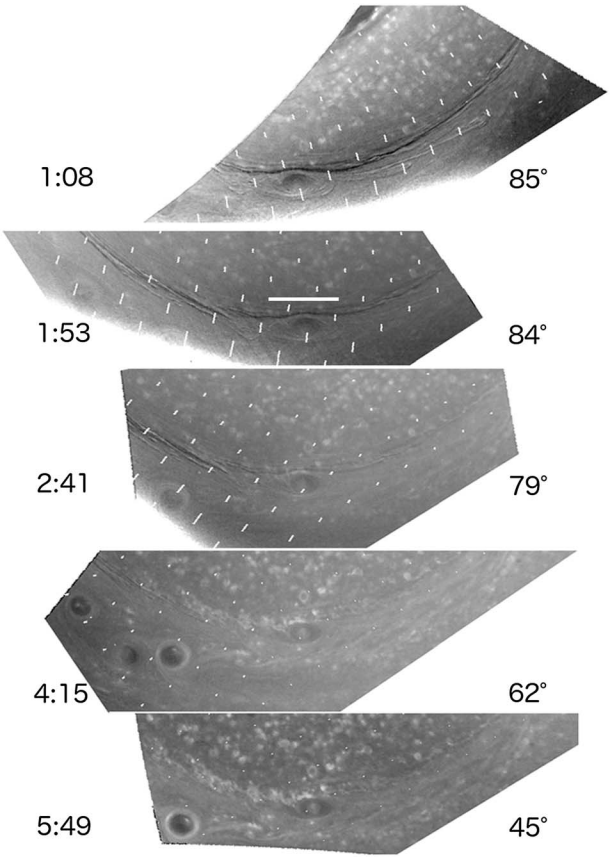

Figure 2. Cloud shadows with the CB2 filter. The cyclone C2 is at the center of each image. The numbers on the left are event times expressed as h:mm on 7 March 2017. The numbers on the right are the solar zenith angles at the center of C2. The features A2, C1, and A3 are visible to the left in the 04:15 image. The scale bar is 5000 km long, and the white lines are the shadows that would be cast by towers 100 km high if they were present. The Sun is in the upper right.

64°N in the top three images as shadows. The fact that the shadows disappear in the lower two images might be due to cloud surfaces whose slopes are between 11° and 28°, which are the complements to the incident angles of the third and fourth images. The cloud heights are less than a few tens of km, i.e., less than a scale height, which is around 35 km at the 100 K/350 mbar level (Fletcher et al., 2016; Schinder et al., 2011).

Figure 3 shows the vortices A1, A2, C1, and A3 at higher resolution than that of Figure 1. Sunlight is coming in from the right, and the white lines are the shadows cast by hypothetical towers 100 km tall. North–south distances between crosses are 4897 km. East–west distances are 12,147 km and 14,043 km at 60°N and 55°N, respectively. Figure S3 shows the same image without the white lines. The region of maximum brightness inside C1 is displaced away from the Sun, indicating a bowl-shaped cloud structure. The opposite is true of A1, A2, and A3, indicating a dome-shaped cloud structure. The bowl shape of the cyclones is consistent with their red color in Figure 1, since both imply downwelling. The dome shape of the anticyclones implies upwelling. These inferences are consistent with Voyager data (Gierasch et al., 1986). As shown in Figure S1, the blue color arises because the anticyclones are dark in CB2 and bright in MT3, which might imply upwelling at the top and downwelling at the bottom. Such a reversal was proposed for Jupiter based on lightning (Ingersoll et al., 2000; Showman & de Pater, 2005) and for Saturn based on chemical tracers (Fletcher et al., 2011). There are other explanations as well, and a full discussion is beyond the scope of this paper.

4. Filaments and Cumulus

Figure 3 shows filaments smoothly interleaved with vortices of the ACA system. Typical widths of the filaments are 200 km, and typical lengths are 20,000 km. The longest filaments in Figure 3 go from the left edge of the image to the right edge, a distance of 17,000 km, without breaking up or losing contrast. They seem to originate inside the vortices and spiral outwards, as with A2 and A3, which rotate clockwise in Figure 3. The coherence of the filaments over long distances gives the impression of a laminar flow. Filaments are common on the southern edge of the high-cloud region at 64°N, as shown in Figure 1. They are ubiquitous in the high-resolution movie taken during the first proximal orbit on 26 April 2017, and they are visible in all filters. The web site is https://www.nasa.gov/feature/jpl/new-movie-shows-cassinis-first-dive-over-saturn. A compressed version named PIA21441 is available in the JPL Photojournal at https://photojournal.jpl.nasa.gov/targetFamily/Saturn.

Figure 4 shows some of the images taken on the 11th proximal orbit, which took place on 29 June 2017. They were taken in the CB2 filter, which gave higher contrast than the CLR filter. Neither filter is especially sensitive to semi-transparent clouds at high altitude, as the methane filters are. Nevertheless, both filaments and cumulus are visible in the images, indicating either that they are not at high altitude or are not optically thin. In other words, the filaments and cumulus are tropospheric phenomena, although their precise altitude is uncertain. Cumulus clouds at 8°S appear in Figure S4 of the supporting information.

The cumulus clouds look pink in the methane filter image of Figure 1, indicating they are deeper than the haze, which looks white. The fact that they are visible at all means that the white clouds are not optically thick at all wavelengths. Both filaments and cumulus clouds are visible in the CB2 and CLR filters, and in Figure 4 the filament strands cross over the cumulus clouds. Thus, it appears that the cumulus clouds are below the filamentary clouds, which are below the semi-transparent clouds and haze that look white in Figure 1.

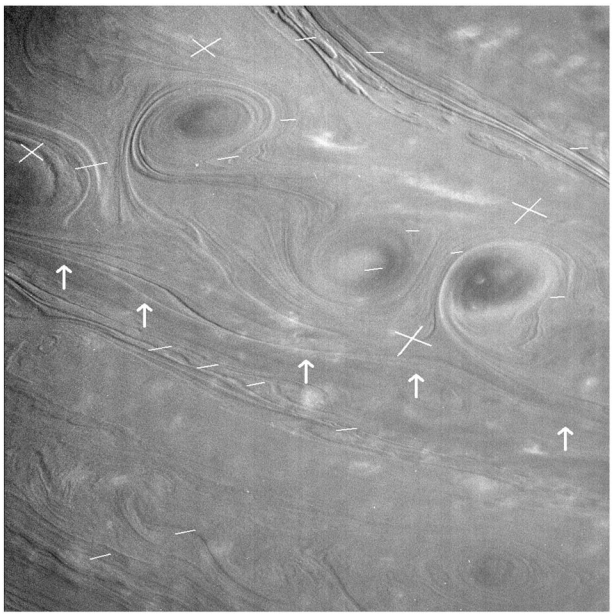

Figure 3. Filaments in a CB2 image taken with the NAC on 27 March 2016 at 20 km per pixel resolution. From left to right, the prominent features are A1, A2, C1, and A3. The crosses are at 55°N and 60°N and at 155°W and 180°W. The Sun is to the right, and the white lines are the shadows that would be cast by towers 100 km tall. The bold arrows point to a filament that crosses the entire image, a distance of 17,000 km. This image without the graphics overlay is Figure S3 of the supporting information.

Figure 5 shows details of a cumulus cloud. The resolution is 0.5 km per pixel, and to the best of our knowledge this resolution is as high as that for any image taken of the planet. The image is about 400 km from the left corner to the right corner. All the images discussed so far are of the northern hemisphere in direct sunlight. Figure 5 is part of a cloud band that circles the planet at 20°S.

5. Dissipation of Kinetic Energy

The coherence of the filaments over long distances allows one to place upper bounds on the horizontal diffusivity and energy dissipation. Consider a bundle of filaments streaming away from their source at speed u in a direction x. The bundle has dimension s in the cross-stream direction y, where s might be the spacing between adjacent filaments. We use the fact that *s* is much less than the length of the filaments. Let *b* (x, y) be the brightness contrast between filaments. Treat *b* (x, y) as an advecting, diffusing fluid in steady state:

$$\frac{db}{dt} = u\frac{\partial b}{\partial x} = D\nabla^2 b \approx D\frac{\partial^2 b}{\partial y^2} = -k^2 Db \tag{1}$$

Here *D* is the diffusivity and *k* is the wavenumber $2\pi/s$ in the cross-stream direction. The equation has a solution *b* (x, y) = *b* (0, y)exp($-k^2Dx/u$). The contrast decays downstream over a characteristic distance $u/(k^2D)$. If the filaments remain coherent over a distance of 20,000 km and the spacing between them is 200 km, with a velocity of 20 m s^{-1}, then the diffusivity *D* is 1013 m^2 s^{-1}. The velocity estimate comes from del Rio-Gaztelurrutia et al. (2018), their Figure 1, which shows the ACA nestled between two eastward jets and almost filling the space between them. That figure is reproduced as Figure S5 in the supporting information of the present paper. The filaments seem to originate inside the vortices and stretch out downstream as noted in Figure 3. Different parts of the vortices are moving at different speeds relative to the ambient flow, and 20 m s^{-1} is a typical differential velocity.

If we further assume that the kinematic viscosity ν is the same order of magnitude as the diffusivity *D*, we can solve for the rate at which the two jets in Figure 1 of del Rio-Gaztelurrutia et al. (2018) are losing kinetic energy. The equation is the same as (1) except we interpret *b* as the kinetic energy per unit mass and the term on the right as the dissipation ε in units of m^2 s^{-3}, or W kg^{-1}. The wavenumber k is now 2π divided by the jet spacing, which is about 6200 km according to Figure 1 of del Rio-Gaztelurrutia et al. (2018), and the velocity from which the kinetic energy is computed is still 20 m s^{-1}. Thus, the dissipation is

$$\varepsilon = \nu\, k^2\, u^2 \approx D\, k^2\, u^2 \approx 4 \times 10^{-7}\ m^2\ s^{-3} \tag{2}$$

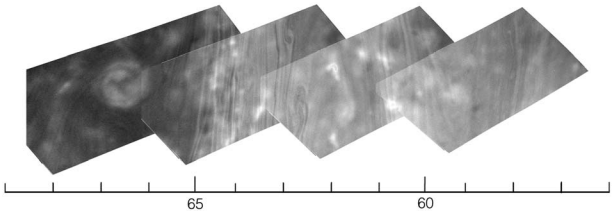

Figure 4. Images in the CB2 filter taken during Cassini's north-to-south dive through the ring plane on 29 June 2017. The latitude scale is at the bottom, and the resolution is 2.4 km/pixel. The filaments at 64°N are the same as those at the southern edge of the haze-covered band in Figure 1. The vortex at 67°N is at the same latitude as A4 and A5 in Figure 1, but identification is hampered by the irregular east–west motion of vortices at this latitude. Clouds with cumulus morphology are visible at all latitudes. Examples of dark filaments covering brighter cumulus clouds occur at latitudes of 60.1°, 60.9°, 63.0°, 63.4°, and 64.6°.

This is a very low dissipation. For Saturn's jet streams the conversion from eddy kinetic energy to zonal mean kinetic energy is ~4×10^{-5} m^2 s^{-3} (Del Genio et al., 2007). For Jupiter the number is ~10^{-4} m^2 s^{-3} (Salyk et al., 2006). For Earth, the global annual-mean dissipation is 1.8×10^{-4} m^2 s^{-3} (Peixoto & Oort, 1992). The number in (2) is highly uncertain, perhaps by an order of magnitude. The low value is implied by the laminar appearance of the high-resolution images, although it might apply only in the upper troposphere, above the main jet streams.

Dissipation arising from vertical wind shear might also contribute to the downstream decay of filaments. For example, Kelvin-Helmholtz (KH) instabilities create transverse disturbances relative to the mean flow.

Figure 5. Cumulus cloud at 20°S. The scale bar is 100 km, and the resolution is 0.5 km per pixel. The image was taken with the CB2 filter in the WAC and is part of the north–south dive through the ring plane on 29 June 2017. This image was taken 45 minutes after the first image in Figure 4.

However, KH instabilities require the Richardson number be less than ¼, and we argue in the SI that above the 0.5 bar pressure level it is greater than 10. The argument involves combining observations of the vertical temperature gradient (Fletcher et al., 2016) with the assumption that the 20 m s^{-1} wind speed difference is spread over one pressure scale height, H ≈35 km.

Vervack and Moses (2015) use photochemical models fitted to Cassini ultraviolet spectrometer (UVIS) data to estimate the vertical diffusivity (their K_{zz} on page 145). They get D = 5 x 10^{-2} m^2 s^{-1} in the pressure range 100 $\leq P <$ 640 mbar. To estimate ε we use Equation (2) with vertical wavenumber k = π/(2H) based on the assumption u (z) = u_0 sin(πz/(2H)) and H = 35 km, where z = 0 is the assumed level of no motion. Then with D = 5 x 10^{-2} m^2 s^{-1} and u_0 = 20 m s^{-1} one obtains ε≈4 x 10^{-8} m^2 s^{-3} for the vertical dissipation, which is an order of magnitude less than the horizontal dissipation given in Equation (2). One expects the horizontal dissipation to be larger than the vertical dissipation, because the latter is inhibited by the stable stratification in the upper troposphere.

6. Conclusions and Questions

Cassini images suggest that filaments and cumulus are the dominant discrete cloud types at scales of 1–10 km, at least at high northern latitudes. Haze at 60–250 mbar overlies the filaments, which overlie the cumulus clouds. From the coherence of the filaments over large horizontal distances, we estimate the dissipation rate ε for the upper troposphere as 4 x 10^{-7} m^2 s^{-3}, which is an extremely low value compared to Jupiter and Earth. It is possible that this low value applies only to the stable layers above the 0.5 bar level and the dissipation is larger at deeper levels.

There are many unanswered questions. What precise altitudes are we looking at in these images? Why are the haze layers confined to particular latitudes, e.g., 64°N - 74°N? Why are the filaments most prevalent at particular latitudes, e.g., at 64°N? What is the relation between the cumulus clouds and convection of heat from below? Why does Saturn have such laminar flow structures in the upper troposphere, and what controls the turbulent dissipation rate? Is it low simply because the radiative heat fluxes are low compared to those on Earth and Jupiter?

Our data provide a glimpse of processes at smaller scales than ever seen before on Saturn. They could be used in conjunction with cloud-resolving models, which will soon be extended from Earth to the giant planets. Questions such models address include the role of convection in transporting heat from below, convective aggregation and interaction with the large-scale flow, and turbulent dissipation - its maintenance and its role in the atmospheric circulation.

Acknowledgments
This work was partly conducted at the Jet Propulsion Laboratory (JPL) under contract with the National Aeronautics and Space Administration (NASA). API and SPE were partly supported by the National Science Foundation (NSF Grant 1411952). The data are in the NASA Planetary Data System. Image numbers are provided in the supporting information.

References

Antunano, A., del Rio-Gaztelurrutia, T., Sanchez-Lavega, A., & Rodriguez-Aseguinolaza, J. (2018). Cloud morphology and dynamics in Saturn's northern polar region. *Icarus*, *299*, 117–132. https://doi.org/10.1016/j.icarus.2017.07.017

Del Genio, A. D., Barbara, J. M., Ferrier, J., Ingersoll, A. P., West, R. A., Vasavada, A. R., et al. (2007). Saturn eddy momentum fluxes and convection: First estimates from Cassini images. *Icarus*, *189*(2), 479–492. https://doi.org/10.1016/j.icarus.2007.02.013

del Rio-Gaztelurrutia, T., Sánchez-Lavega, A., Antuñano, A., Legarreta, J., García-Melendo, E., Sayanagi, K. M., et al. (2018). A planetary-scale disturbance in a long living three vortex coupled system in Saturn's atmosphere. *Icarus*, *302*, 499–513. https://doi.org/10.1016/j.icarus.2017.11.029

Dyudina, U. A., Ingersoll, A. P., Ewald, S. P., Vasavada, A. R., West, R. A., Baines, K. H., et al. (2009). Saturn's south polar vortex compared to other large vortices in the solar system. *Icarus*, *202*(1), 240–248. https://doi.org/10.1016/j.icarus.2009.02.014

Fletcher, L. N., Baines, K. H., Momary, T. W., Showman, A. P., Irwin, P. G. J., Orton, G. S., et al. (2011). Saturn's tropospheric composition and clouds from Cassini/VIMS 4.6-5.1 mu nightside spectroscopy. *Icarus*, *214*, 510–533. https://doi.org/10.1016/j.icarus.2011.06.006

Fletcher, L. N., Irwin, P. G. J., Achterberg, R. K., Orton, G. S., & Flasar, F. M. (2016). Seasonal variability of Saturn's tropospheric temperatures, winds and Para-H-2 from Cassini far-IR spectroscopy. *Icarus*, *264*, 137–159. https://doi.org/10.1016/j.icarus.2015.09.009

Garcia-Melendo, E., Arregi, J., Rojas, J. F., Hueso, R., Barrado-Izagirre, N., Gomez-Forrellad, J. M., et al. (2011). Dynamics of Jupiter's equatorial region at cloud top level from Cassini and HST images. *Icarus*, *211*(2), 1242–1257. https://doi.org/10.1016/j.icarus.2010.11.020

Garcia-Melendo, E., Sanchez-Lavega, A., Rojas, J. F., Perez-Hoyos, S., & Hueso, R. (2009). Vertical shears in Saturn's eastward jets at cloud level. *Icarus*, *201*(2), 818–820. https://doi.org/10.1016/j.icarus.2009.02.022

Gierasch, P. J., Conrath, B. J., & Magalhaes, J. A. (1986). Zonal mean properties of Jupiter upper troposphaere from voyager infrared observations. *Icarus*, *67*(3), 456–483. https://doi.org/10.1016/0019-1035(86)90125-9

Ingersoll, A. P., Gierasch, P. J., Banfield, D., Vasavada, A. R., & the Galileo Imaging Team (2000). Moist convection as an energy source for the large-scale motions in Jupiter's atmosphere. *Nature*, *403*(6770), 630–632. https://doi.org/10.1038/35001021

Peixoto, J. P., & Oort, A. H. (1992). *Physics of Climate*. New York: Amer. Inst. Phys.

Porco, C. C., West, R. A., Squyres, S., Mcewen, A., Thomas, P., Murray, C. D., et al. (2004). Cassini imaging science: Instrument characteristics and anticipated scientific investigations at Saturn. *Space Science Reviews*, *115*(1–4), 363–497. https://doi.org/10.1007/s11214-004-1456-7

Salyk, C., Ingersoll, A. P., Lorre, J., Vasavada, A., & Del Genio, A. D. (2006). Interaction between eddies and mean flow in Jupiter's atmosphere: Analysis of Cassini imaging data. *Icarus*, *185*(2), 430–442. https://doi.org/10.1016/j.icarus.2006.08.007

Sanz-Requena, J. F., Perez-Hoyos, S., Sanchez-Lavega, A., Antunano, A., & Irwin, P. G. J. (2018). Haze and cloud structure of Saturn's north pole and hexagon wave from Cassini/ISS imaging. *Icarus*, *305*, 284–300. https://doi.org/10.1016/j.icarus.2017.12.043

Schinder, P. J., Flasar, F. M., Marouf, E. A., French, R. G., McGhee, C. A., Kliore, A. J., et al. (2011). Saturn's equatorial oscillation: Evidence of descending thermal structure from Cassini radio occultations. *Geophysical Research Letters*, *38*, L08205. https://doi.org/10.1029/2011gl047191

Showman, A. P., & de Pater, I. (2005). Dynamical implications of Jupiter's tropospheric ammonia abundance. *Icarus*, *174*(1), 192–204. https://doi.org/10.1016/j.icarus.2004.10.004

Vasavada, A. R., Horst, S. M., Kennedy, M. R., Ingersoll, A. P., Porco, C. C., Del Genio, A. D., & West, R. A. (2006). Cassini imaging of Saturn: Southern hemisphere winds and vortices. *Journal of Geophysical Research*, *111*, E05004. https://doi.org/10.1029/2005je002563

Vervack, R. J., & Moses, J. I. (2015). Saturn's upper atmosphere during the voyager era: Reanalysis and modeling of the UVS occultations. *Icarus*, *258*, 135–163. https://doi.org/10.1016/j.icarus.2015.06.007

West, R. A., Baines, K. H., Karkoschka, E., & Sanchez-Lavega, A. (2009). Clouds and aerosols in Saturn's atmosphere. In M. K. Doughterty, L. W. Esposito, & S. M. Krimigis (Eds.), *Saturn from Cassini-Huygens* (pp. 161–179). Dordrecht, Netherlands: Springer. https://doi.org/10.1007/978-1-4020-9217-6_7